





## ORIGINAL ARTICLE

# Cell-Specific Loss of SNAP25 from Cortical Projection Neurons Allows Normal Development but Causes Subsequent Neurodegeneration

Anna Hoerder-Suabedissen <sup>1</sup>, Kim V. Korrell<sup>1</sup>, Shuichi Hayashi<sup>1</sup>, Alexander Jeans<sup>2</sup>, Denise M.O. Ramirez<sup>3,6</sup>, Eleanor Grant<sup>1</sup>, Helen C. Christian<sup>1</sup>, Ege T. Kavalali<sup>3,4</sup>, Michael C. Wilson<sup>5</sup> and Zoltán Molnár <sup>1</sup>

<sup>1</sup>Department of Physiology, Anatomy and Genetics, University of Oxford, South Parks Road, Oxford, OX1 3QX, UK, <sup>2</sup>Department of Pharmacology, Mansfield Road, Oxford, OX1 3QT, UK, <sup>3</sup>Department of Neuroscience, University of Texas Southwestern Medical Center, 5323 Harry Hines Blvd., Dallas, TX 75390, USA, <sup>4</sup>Department of Physiology, University of Texas Southwestern Medical Center, 5323 Harry Hines Blvd., Dallas, TX 75390, USA, <sup>5</sup>Department of Neurosciences, University of New Mexico, Albuquerque, NM 87131-0001, USA and <sup>6</sup>Present address: Department of Neurology and Neurotherapeutics, University of Texas Southwestern Medical Center, 5323 Harry Hines Blvd., Dallas, TX 75390-8813, USA

Address correspondence to Anna Hoerder-Suabedissen and Zoltán Molnár. Email: anna.hoerder-suabedissen@dpag.ox.ac.uk (A.H-S); zoltan.molnar@dpag.ox.ac.uk (Z.M.)  [orcid.org/0000-0003-1953-7871](https://orcid.org/0000-0003-1953-7871),  [orcid.org/0000-0002-6852-6004](https://orcid.org/0000-0002-6852-6004)

## Abstract

Synaptosomal associated protein 25 kDa (SNAP25) is an essential component of the SNARE complex regulating synaptic vesicle fusion. SNAP25 deficiency has been implicated in a variety of cognitive disorders. We ablated SNAP25 from selected neuronal populations by generating a transgenic mouse (B6-Snap25tm3mcw (Snap25-flox)) with LoxP sites flanking exon5a/5b. In the presence of Cre-recombinase, Snap25-flox is recombined to a truncated transcript. Evoked synaptic vesicle release is severely reduced in Snap25 conditional knockout (cKO) neurons as shown by live cell imaging of synaptic vesicle fusion and whole cell patch clamp recordings in cultured hippocampal neurons. We studied Snap25 cKO in subsets of cortical projection neurons in vivo (L5—Rbp4-Cre; L6—Ntsr1-Cre; L6b—Drd1a-Cre). cKO neurons develop normal axonal projections, but axons are not maintained appropriately, showing signs of swelling, fragmentation and eventually complete absence. Onset and progression of degeneration are dependent on the neuron type, with L5 cells showing the earliest and most severe axonal loss. Ultrastructural examination revealed that cKO neurites contain autophagosome/lysosome-like structures. Markers of inflammation such as Iba1 and lipofuscin are increased only in adult cKO cortex. Snap25 cKO can provide a model to study genetic interactions with environmental influences in several disorders.

**Key words:** Drd1a-Cre, neurodegeneration, Ntsr1-Cre, Rbp4-Cre, SNAP25

## Introduction

Neurons communicate with each other through the regulated release of synaptic vesicles. The soluble N-ethylmaleimide fusion

protein attachment protein receptor (SNARE) complex is essential for the regulation of this vesicular release (Rizo and Südhof 2012). Synaptosomal associated protein of 25 kDa (SNAP25) is a

component of the SNARE complex in neurons. SNAP25 is essential for action-potential (AP) evoked neurotransmitter release at both neuromuscular junctions and central nervous system synapses (Washbourne et al. 2002; Bronk et al. 2007).

*Snap25*<sup>-/-</sup> mice die at birth, have reduced embryonic size and are immobile, but their nervous system develops histologically normally until embryonic day (E)19 (Molnár et al. 2002; Washbourne et al. 2002). *Snap25*<sup>+/-</sup> mice show no overt behavioral phenotypes (Washbourne et al. 2002) despite a 40% decrease in SNAP25 protein levels (Washbourne et al. 2002; Sharma et al. 2012). SNAP25-KO cortical and thalamic axons extend with normal developmental trajectories and target their normal destinations and form immature synapses in vitro and in vivo (Molnár et al. 2002; Washbourne et al. 2002). Similarly, thalamic afferents target cortical layer 4 cells normally and begin to form normal branches in organotypic cocultures of SNAP25 deficient thalamic explants and wild-type cortices (Blakey et al. 2012). Cultured *Snap25*<sup>-/-</sup> hippocampal cells display spontaneous miniature excitatory postsynaptic currents (mEPSCs) in the presence of TTX that are of normal amplitude but occur at reduced frequency (Washbourne et al. 2002).

SNAP25 deficiency has been implicated in a variety of neurodevelopmental disorders and may contribute to genetic interactions with environmental influences on such disorders. *Snap25* is a candidate susceptibility gene for schizophrenia (Ayalew et al. 2012; Dai et al. 2014) and attention deficit hyperactivity disorder (Faraone and Khan 2006). *Blind-drunk* (*Bdr*) mice with a dominant negative point mutation in *Snap25* survive to adulthood, but display characteristic ataxic gait, and prepulse inhibition deficits without overt neuropathology (Jeans et al. 2007). Additionally, *Bdr* mice show disrupted circadian rhythms reminiscent of the sleep disruptions observed in schizophrenia (Oliver et al. 2012). *Snap25*<sup>+/-</sup> mice prenatally exposed to nicotine exhibit hyperactivity and deficits in social interaction as adults (Baca et al. 2013). Coloboma (*Cb*) mice, in which a section of chromosome 2 including *Snap25* is deleted, are spontaneously hyperactive (Hess et al. 1992).

SNAP25 may also play a role in neurodegenerative disorders. In transgenic mouse models of Parkinson's disease, overexpression of human  $\alpha$ -synuclein results in protein aggregates including SNAP-25, and reduced exocytosis in PC12 cells and dopaminergic neurons (Garcia-Reitböck et al. 2010). Reduction in SNAP25 levels was observed in prefrontal cortex of Alzheimer's disease patients (Bereczki et al. 2016). Lastly, the lethal cysteine-string protein alpha (*CSP $\alpha$* ) KO is accompanied by reductions in SNAP25 and can be rescued by increasing SNAP25 levels (Sharma et al. 2012).

Here we analyzed a cell-type specific knock-down of SNAP25 in *Rbp4*-expressing cortical L5 cells in an otherwise wild-type brain. In *Rbp4-Cre;Snap25-flox/flox;Ai14-tdTomato* mice, long-range subcortical axons develop normally. By 3 weeks after birth, axons begin to show signs of fragmentation and eventually disappear entirely over the following month. *Cre*<sup>+</sup> cell density in cortical L5 does not decrease in the same time frame, nor do the animals show any obvious signs of motor deficits at this age. However, from 4 to 5 months of age, most cKO mice develop hindlimb clasp. Finally, by 8 months of age, cortical *Cre*<sup>+</sup> cell density is decreased, remaining neurites show signs of autophagosomes and markers of inflammation such as *Iba1*<sup>+</sup> cells and lipofuscin deposits are increased. Axonal fragmentation and cell death are also observed in *Ntsr1-Cre* expressing cortical L6 or *Drd1a-Cre* expressing L6b cells in the presence of *Snap25flox/flox*, albeit on a much slower time-scale.

## Methods

### Breeding and Maintenance of Transgenic Mice

All experiments were performed under a valid Animals (Scientific Procedures) Act project license and with local ethical approval (UK) or in accordance with the National Institutes of Health Guide for Care and Use of Laboratory Animals (USA).

*B6-Snap25tm3mcw* (*Snap25*<sup>fl/fl</sup> and *Snap25*<sup>fl/+</sup>) mice were obtained from University of New Mexico (Michael C. Wilson) and bred to homozygosity. Three *Cre*-recombinase expressing strains (*Tg(Rbp4-cre)KL100Gsat/Mmucd* (*Rbp4-Cre*; Jackson Laboratories); *Tg(Ntsr1-cre)GN220Gsat* (*Ntsr1-Cre*; Jackson Laboratories) and *Tg(Drd1a-cre)FK164Gsat/Mmucd* (*Drd1a-Cre*; MMRRC)) and *Snap25*<sup>fl/fl</sup> were crossed to *B6;129S6-Gt(ROSA)26Sortm14(CAG-tdTomato)Hze/J* (*Ai14*) mice. Control mice were obtained by crossing *Cre*<sup>+</sup>; *Ai14/Ai14* females with *Ai14/Ai14* males. Conditional knockout and heterozygous knockout mice were obtained by crossing *Cre*<sup>+</sup>; *Snap25*<sup>fl/+</sup>; *Ai14* females (*Rbp4-Cre*) or *Cre*<sup>+</sup>; *Snap25*<sup>fl/fl</sup>; *Ai14* females (*Ntsr1-Cre* and *Drd1a-Cre*) with *Snap25*<sup>fl/fl</sup>; *Ai14/Ai14* males.

Animals were weighed on standard digital scales (accuracy 0.1 g) at P14 and twelve weeks (*Rbp4-Cre*) and 8 months of age (all strains). Additional health observations were noted as part of routine animal husbandry.

### Axonal Projection Development and Maintenance In Vivo

*Cre*<sup>+</sup>; *Ai14;Snap25*<sup>+/+</sup> and *Cre*<sup>+</sup>; *Ai14;Snap25*<sup>fl/+</sup> (*Ctrl*), or *Cre*<sup>+</sup>; *Ai14;Snap25*<sup>fl/fl</sup> (cKO) mice at various postnatal ages were perfusion fixed with 4% formaldehyde (F8775; Sigma-Aldrich) in 0.1 M PBS, and dissected brains postfixed in the same for 24–48 h at 4 °C. See Supplementary Table S1 for a summary of the brains and ages used. Brains were sectioned coronally at 50  $\mu$ m on a vibrating microtome (Leica, VT1000S), counterstained with 4',6'-diamidino-2'-phenylindole dihydrochloride (DAPI) and mounted. Images were acquired on a confocal laser scanning microscope (Zeiss LSM710), and collapsed image stacks analyzed for continuous labeling of cellular processes (axons and dendrites) in regions of sparse projections. Tile-scans through the entire cortical depth were used for quantification of *Cre*<sup>+</sup>; *Ai14*-labeled cells. Cell count data is displayed in box and whisker plots, where the top and bottom of each box represent the 25th and 75th percentiles of the data, respectively, while whiskers represent the extremes of the data range. The short line in the middle of each box represents the median.

To determine axon integrity in the spinal cord, cervical spinal cord was dissected out and the *tdTomato* positive area (dorsal corticospinal tract) flat-mounted longitudinally (P21–P44, *n* = 2–4/genotype) or cut coronally (P80, *n* = 3/genotype).

### Immunohistochemistry to Detect Changes in Synaptic and Inflammatory Markers

To determine the percentage of L5 neurons expressing *Rbp4-Cre::tdTomato*, 50  $\mu$ m coronal sections of *n* = 3 P6 *Rbp4-Cre;Ai14* fixed brains were stained with mouse anti-NeuN antibody (1:1000; MAB377; Chemicon). To detect changes in VGLUT1+ synapses in Po thalamus, 50  $\mu$ m coronal sections of *n* = 3 P28 *Rbp4-Cre;Ai14;Snap25*<sup>+/+</sup> (*Ctrl*), or *Rbp4-Cre;Ai14;Snap25*<sup>fl/fl</sup> (cKO) fixed brains were stained with guinea-pig anti-VGLUT1 antibody (1:10 000; Ab5905; Millipore). To detect changes in inflammatory processes, coronal sections of *n* = 3 P48 and *n* = 5 8-month-old

brains of *Rbp4-Cre;Ai1;Snap25<sup>+/+</sup>* (Ctrl), or *Rbp4-Cre;Ai14;Snap25<sup>fl/fl</sup>* (cKO) mice were stained with goat anti-Iba1 antibody (1:500; ab5076; Abcam). Briefly, sections were incubated in blocking solution (2% donkey serum and 0.1–0.2% Triton-X100 in 0.1 M PBS) for 2 h before incubation with the primary antibody in blocking solution overnight (NeuN and Iba1) or for 72 h (VGLUT1) at 4°C. The primary antibody was revealed by incubating with donkey antimouse-AlexaFluor488 (1:500), donkey antigoat-AlexaFluor488 (1:500) or donkey-antiguineapig AlexaFluor488 (1:500) for 2 h at room temperature, before counterstaining with DAPI.

#### Quantification of VGLUT1+ Synapses

Confocal image stacks using  $\times 63$  objective were acquired of VGLUT1+ stained Po thalamus in P28 cKO and control brains, with identical settings for all brain sections. The 15 tdTomato+ presumed boutons were outlined in ImageJ on a single z-plane, and the mean pixel intensity of the VGLUT1+ signal was determined in the corresponding region. Mean VGLUT1 pixel intensity was normalized by subtracting the mean signal intensity across the whole image. Data is displayed in box and whisker plots, where the top and bottom of each box represent the 25th and 75th percentiles of the data, respectively, while whiskers represent the extremes of the data range, and the cross is the mean.

#### Electron Microscopy Sample Preparation and Image Acquisition

Electron microscopy was performed on somatosensory cortex of *Rbp4-Cre;Ai14;Snap25<sup>fl/fl</sup>* (Ctrl,  $n = 3$  brains) and *Rbp4-Cre;Ai14;Snap25<sup>fl/fl</sup>* (cKO,  $n = 4$  brains) 8-month-old adult mice. The mice were perfused transcardially with  $\sim 15$  mL of fixative containing 4% formaldehyde (Sigma-Aldrich) and 0.2% glutaraldehyde (TAAB) in 0.1 M PBS. Dissected brains were postfixed in PBS containing 4% formaldehyde and 0.2% glutaraldehyde overnight at 4°C. The fixed brains were cut serially in 80  $\mu\text{m}$ -thick coronal sections on a vibrating microtome (Leica, VT1000S), and tissue pieces containing somatosensory cortex were dissected out under a fluorescence microscope (MZFLIII, Leica). Tissue pieces containing somatosensory cortex were stained with 2% uranyl acetate (British Drug Houses) in 0.1 M sodium acetate buffer for 45 min–1 h. After dehydration through a graded series of methyl alcohol (70%, 90%, and absolute) at  $-20^\circ\text{C}$ , the tissues were embedded in LR gold resin (Agar Scientific) containing 0.5% benzil (Agar Scientific) under UV light for 16–18 h at  $-20^\circ\text{C}$ . Ultra-thin sections (70–90 nm) were prepared and mounted on formvar-coated 200-mesh nickel grids (Agar Scientific). For immunolabelling, sections were blocked with 1% chicken egg albumin (Sigma-Aldrich) in PBS and incubated with rabbit anti-red fluorescent protein (RFP) antibody (1:500, PM005, MBL international) for 2 h and then with 20 nm gold particle-conjugated goat antirabbit (1:50, BBI solutions) for 1 h. For negative control sections, the primary antibody was omitted. Immunolabelled sections were postfixed with 1% glutaraldehyde for 10 min. All the sections were lightly counterstained with 2% uranyl acetate and lead citrate solution containing 2.77% lead nitrate (British Drug Houses) and examined on a JEOL 1010 transmission electron microscope (JEOL) fitted with an Orius digital camera (Gatan).

#### Data Analysis and Image Processing

Manual cell counts were obtained from at least  $n = 3$  different brains. For Lipofuscin/autofluorescence spot quantification, a

custom optimized analysis pipeline in Cell Profiler (Lamprecht et al. 2007) was used. Unless stated otherwise, t-tests with unequal variance were used to determine statistical significance.

Images were intensity and contrast adjusted using Photoshop, and some were converted to greyscale. Figures were assembled using Photoshop.

## Results

To study the development and maintenance of long-range axonal projections from a presynaptically “silenced” subset of cortical projection neurons in an otherwise wild-type brain, we generated *Rbp4-Cre;Snap25-flox/flox;Ai14-tdTomato* mice. *Rbp4-Cre* is expressed in L5, subcortically projecting pyramidal cells, a small fraction of cortical L6b cells and dentate gyrus neurons (Gong et al. 2007; Grant et al. 2016; see Figs 1 and 2) as well as in selected thalamic nuclei and superior colliculus (Grant et al. 2016). When crossed with the STOP-floxed tdTomato reporter line Ai14, labeled axons are evident in the thalamus at birth but innervation density of higher order thalamic nuclei increases strongly throughout the first postnatal week (Grant et al. 2016; see Fig. 1). In the *Rbp4-Cre;Snap25-flox/flox;Ai14-tdTomato* mouse, exon5a/5b is efficiently excised in Cre-expressing cells of the dentate gyrus and SNAP25 is absent from the mossy fiber pathway of “silenced” brains (Supplementary Fig. S1). B6-Snap25tm3mcw (*Snap25-flox*) has been previously used to effectively silence somatostatin-expressing interneurons in the developing cortex (Marques-Smith et al. 2016) and dentate gyrus granule cells (Gustus et al., submitted). For a more detailed description of the generation of the *Snap25-flox* transgenic mouse (Supplementary Fig. 1), and additional validation including quantitative analysis of presynaptic vesicle release in cultured hippocampal neurons using pHluorin imaging of vesicle fusion (Supplementary Fig. S2) or electrophysiological recordings of cultured inhibitory interneurons (Supplementary Fig. S3), please see the Supplementary text and supplementary figures.

#### *Snap25* cKO in vivo allows normal development of long-range cortical projections but results in impaired axon integrity with age

To study the effect of “silencing” a subgroup of cortical projection neurons, *Snap25<sup>fl/fl</sup>* mice were crossed with *Rbp4-Cre;Ai14* mice. In *Rbp4-Cre;Ai14* (control) brains, labeled cells are detectable in cortex from E16 (data not shown). We determined that *Rbp4-Cre::tdTomato* labels 15% of NeuN+ cells in L5 at P6 ( $14.54 \pm 3.9$ , mean  $\pm$  standard deviation [s.d.],  $n = 3$  brains). *Rbp4-Cre+* L5 pyramidal neurons project to several targets, including the contralateral hemisphere via the corpus callosum, the higher order thalamic nuclei via the internal capsule and the basal pons and spinal cord via the cerebral peduncle (Figs 1 and 2). Additional expression was identified in the cerebellum including Purkinje and granule cells, though this was highly variable between animals (data not shown).

tdTomato+ cells are abundant in L5 of *Rbp4-Cre;Ai14;Snap25<sup>fl/fl</sup>* (cKO) brains from birth (see Fig. 1A for expression at P2) until 9 months of age (oldest time-point investigated). Axonal projection patterns in cKO brains develop normally between P2 and P8 with no noticeable differences between the control and the silenced projection pathways (Fig. 1). There was no difference in the innervation density in their targets, such as the higher order and midline thalamic nuclei, or the pattern of fasciculation in the cerebral peduncle (Fig. 1C,D') at P8. No



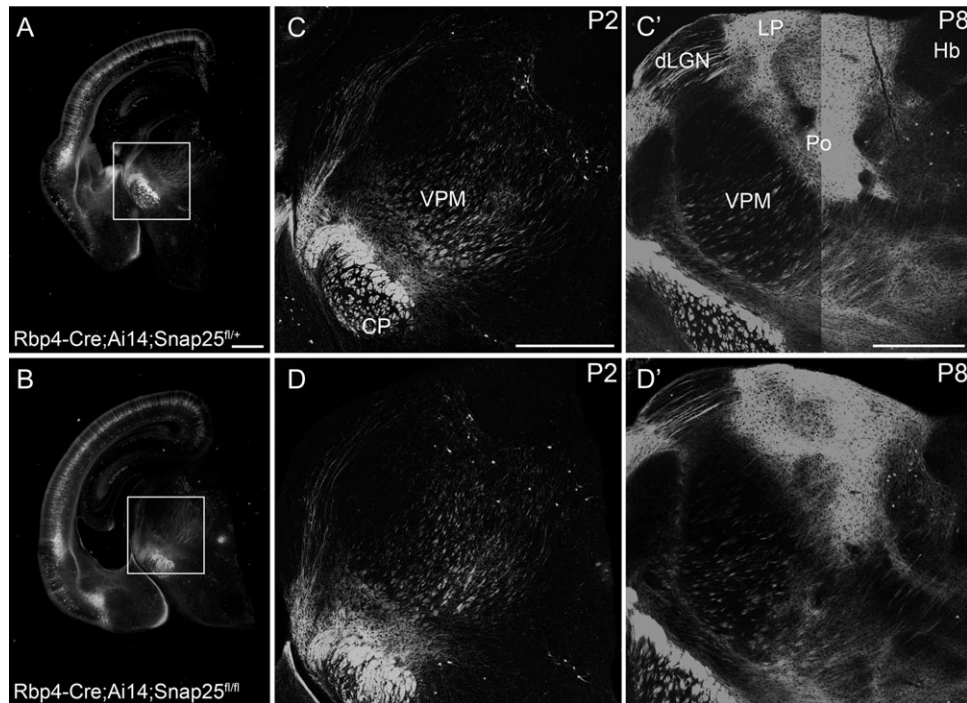


**Figure 1.** In vivo Cre-expression allows normal development of long-range axonal projections in control and “silenced” Rbp4-Cre expressing cortical L5 projection neurons. Epifluorescent (A, B) and laser scanning confocal microscope tiled images of *Rbp4-Cre;Ai14;Snap25<sup>fl/fl</sup>* or *Rbp4-Cre;Ai14;Snap25<sup>fl/fl</sup>* brains. (A, B) images of P2 brains from *Rbp4-Cre;Ai14;Snap25<sup>fl/fl</sup>* or *Rbp4-Cre;Ai14;Snap25<sup>fl/fl</sup>* mice, demonstrating presence of tdTom+ cells in the cortex, and tdTom+ fibers projecting subcortically. Boxed region enlarged in (C, D). (C, D) tiled confocal images of tdTom+ fibers in the thalamus and cerebral peduncle (CP) at P2. While projections in the cerebral peduncle are already very abundant and dense, projections to higher order thalamic nuclei such as posterior (Po) nucleus are barely detectable at this age. (C', D') tiled confocal images of tdTom+ fibers in the thalamus and cerebral peduncle at P8. By this time point, tdTom+ axons course through dorsal lateral geniculate nucleus (dLGN) and form dense terminal arborisations in Po and lateral posterior nucleus (LP). The subcerebral projections extend within the cerebral peduncle. The pattern, intensity and fasciculation patterns appear identical in the *Rbp4-Cre;Ai14;Snap25<sup>fl/fl</sup>* and *Rbp4-Cre;Ai14;Snap25<sup>fl/fl</sup>* brains. Structures normally devoid of L5 fibers such as habenula do not receive inappropriate innervation in the *Rbp4-Cre;Ai14;Snap25<sup>fl/fl</sup>* brain. Note the absence of tdTomato-expression in the dentate gyrus at P2. Scale bars = 500  $\mu$ m. Abbreviations: CP, cerebral peduncle; dLGN, dorsal lateral geniculate nucleus; Hb, habenula; LP, lateral posterior nucleus; Po, posterior nucleus; VPM, ventral posterior medial nucleus.

differences between “silenced” and control brains are obvious at P21 (Fig. 2A,B), but at the beginning of the fourth postnatal week, distal axons in the cervical spinal cord start to appear fragmented (Fig. 3B,B'). Axons in the striatum and traversing through the dorsal lateral geniculate nucleus (dLGN) appear normal at P21 and P35 (Fig. 2D,D',F,F'). By P48, however, axonal integrity is also drastically impaired in the striatum and dLGN (Fig. 2F') compared with control brains (Fig. 2D'). Individual axons in the thalamus are discontinuously labeled and contain large swellings or accumulations of tdTomato protein in cKO brains.

By P28, large and very abundant tdTomato+ punctae are visible in cortex and medial thalamic nuclei including the higher order posterior thalamic nucleus (Po), but axons remain continuous and without major swellings in first order thalamic nuclei. Most of the large tdTomato+ punctae are not hypertrophic synapses, as few of them are VGluT1+, in contrast to the large boutons typically formed by L5 axons in Po (Hoogland et al. 1991; Groh et al. 2014; Fig. 4). However, a few of the tdTomato+ processes in Po are VGluT1+ in “silenced” brains, and they are indistinguishable from those in control brains based on the average VGluT1+ pixel intensity. This suggests that some synapses initially formed, and are then lost in a degenerative process (Fig. 4). Overall, the mean normalized VGluT1+ pixel intensity in regions of tdTomato+ boutons is significantly lower in cKO brains ( $19 \pm 4$  [cKO] vs.  $58 \pm 5$  [ctrl; mean  $\pm$  standard error of the mean (s.e.m.)];  $P < 0.001$ , 2-tailed t-test unequal variance). The presumed

boutons are smaller on average in cKO compared with control brains ( $3.4\text{pix} \pm 0.2$  [cKO] vs.  $4.9\text{pix} \pm 0.3$  [ctrl; mean  $\pm$  s.e.m.];  $P < 0.001$ , 2-tailed t-test unequal variance). Dendrites remain intact throughout the same time period and into much older ages (see Fig. 5A for an example at 8 months of age). Therefore, the abundant tdTomato+ punctae in cortex are assumed to derive from degenerating axons and synapses.

No decrease in the density of labeled L5 somata was apparent in S1 at P21 or P48 ( $P21:58 \pm 8$  [ctrl] vs.  $63 \pm 4$  [cKO] cells;  $P48:64 \pm 15$  [ctrl] vs.  $59 \pm 10$  [cKO] cells; mean  $\pm$  s.d.;  $n = 3$  brains per age and genotype). However, by 8 months of age, a drastic reduction of labeled L5 cells was evident in the cKO brains ( $55 \pm 11$  [ctrl] vs.  $23 \pm 2$  [cKO] cells; mean  $\pm$  s.d.;  $n = 5$  brains per age and genotype; Figs 5D and 7C;  $P < 0.005$  2-tailed t-test with unequal variance).

Ultrastructure of degenerating neurites was investigated in somatosensory cortex of 8-month-old brains. Transmission electron microscopy (TEM) of sections of *Rbp4-Cre;Ai14;Snap25<sup>fl/fl</sup>* cortex immuno-gold-labeled for tdTomato showed tdTomato+ neurites with altered cytoplasmic appearances (Fig. 6A–C,F,G,  $n = 41$  from 4 brains). Specifically, tdTomato+ neurites contained an electron-dense cytoplasm (Fig. 6B,C) closely packed with multivesicular bodies (Fig. 6A'), and numerous vacuoles containing an electron-dense body (Fig. 6A",B",B"). The latter organelles are putative autophagosome/lysosome-like structures (Nixon et al. 2005; Kishi-Itakura et al. 2014), a feature of dystrophic neurites in neurodegenerative diseases such as Alzheimer's disease and its mouse

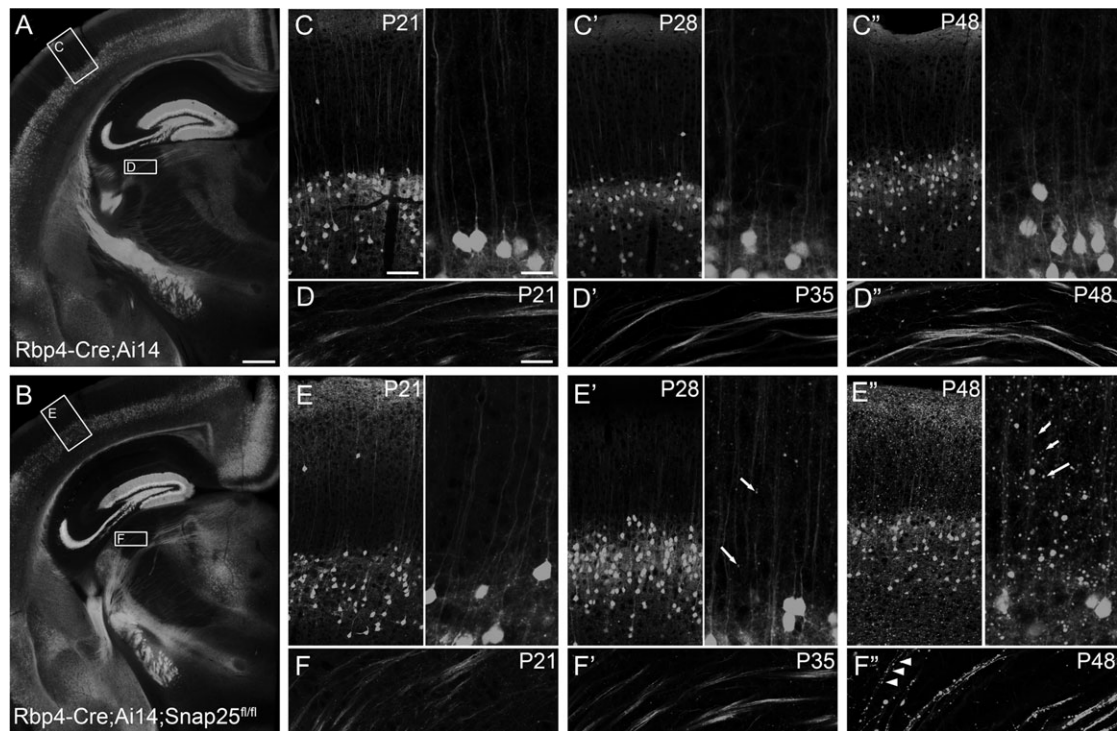


**Figure 2.** Cell-type selective knock-down of SNAP25 in *Rbp4-Cre;Ai14* layer 5 projection neurons elicited axon disintegration from third postnatal week onwards. Epifluorescent (A, B) and laser scanning confocal microscope tiled images of *Rbp4-Cre;Ai14* or *Rbp4-Cre;Ai14;Snap25<sup>fl/fl</sup>* brains. (A) Representative section from a P21 *Rbp4-Cre;Ai14* control brain. (B) All projections have developed normally in the *Rbp4-Cre;Ai14;Snap25<sup>fl/fl</sup>* brain by P21, and no cell groups or major axon bundles are missing compared with control brains. Boxes in (A, B) highlight areas of cerebral cortex and dorsolateral geniculate nucleus (dLGN) shown in panels C–F. (C, E) At P21, control and *Snap25<sup>fl/fl</sup>* tdTomato+ cells in the cortex have developed a mature dendrite and abundant local neuropil. (D, F) tdTomato+ L5 neurons in control and *Rbp4-Cre;Ai14;Snap25<sup>fl/fl</sup>* brains have extended axons through dLGN by P21 without forming synapses there. (C', E') By P28, large tdTomato+ punctae are visible in the *Rbp4-Cre;Ai14;Snap25<sup>fl/fl</sup>* cortex (arrows in E') but not in controls. (D', F') Axons through dLGN remain continuously labeled at P35. (C'', E'') By P48 the cortex of *Rbp4-Cre;Ai14;Snap25<sup>fl/fl</sup>* brains contains many large tdTomato+ swellings (arrows). (D'', F'') Axons in dLGN are discontinuous (arrowheads) and contain large tdTomato+ swellings in *Rbp4-Cre;Ai14;Snap25<sup>fl/fl</sup>* brains, but remain continuous and without swellings in *Rbp4-Cre;Ai14*. Scale bars = 500  $\mu$ m (A, B), 100  $\mu$ m (C, E, left panel), 50  $\mu$ m (D, F), or 25  $\mu$ m (C, E, right panel).

models (Masliah et al. 1996; Nixon et al. 2005; Sanchez-Varo et al. 2012). The number and size of the vacuoles and the electron-density of the cytoplasm varied among the neurites in *Rbp4-Cre;Ai14;Snap25<sup>fl/fl</sup>* cortex, which may reflect varying degrees of degeneration. Such altered ultrastructural appearance was not observed in axons and dendrites of *Rbp4-Cre;Ai14;Snap25<sup>fl/+</sup>* cortex (Fig. 6D,E; more than  $n = 20$  tdTomato+ axons and dendrites for each were observed from 3 brains). Some dystrophic neurites were identified as an axon (Fig. 6F,  $n = 9$ ) or a dendrite (Fig. 6G,  $n = 2$ ) by the presence of asymmetric synaptic structures. The dystrophic axonal boutons in *Rbp4-Cre;Ai14;Snap25<sup>fl/fl</sup>* cortex also contained multivesicular bodies (Fig. 6F,F') and dystrophic dendrites contained denser cytoplasm and vacuoles (Fig. 6G) indicating ongoing neurite degeneration in *Rbp4-Cre;Ai14;Snap25<sup>fl/fl</sup>* at 8 months of age. These features were not observed in axonal boutons and dendrites of *Rbp4-Cre;Ai14;Snap25<sup>fl/+</sup>* cortex (Fig. 6D,E).

Evidence of axonal degeneration is not restricted to L5 pyramidal neurons, but it progresses at different rates in other “silenced” cortical cell populations. In the *Ntsr1-Cre* line, the majority of L6a cells with subcortical axons express Cre-recombinase (Olsen et al. 2012). For several months postnatally, there is no evidence of axon fragmentation in *Ntsr1-Cre;Ai14;Snap25<sup>fl/fl</sup>* mice. However, as in *Rbp4-Cre;Ai14;Snap25<sup>fl/fl</sup>* mice, by 10 months of age, axons in the striatum and thalamus are virtually absent (Fig. 7E'',E'''), and there is a significant reduction in Cre+ cell bodies in cortical layer 6a of motor cortex ( $114.4 \pm 5.8$  [ctrl] vs.  $89.7 \pm 5.8$  [cKO];  $P < 0.05$  2-tailed t-test unequal

variance;  $n = 3$  brains for each genotype, Fig. 7F). In the *Drd1a-Cre* line, Cre-recombinase is expressed in L6b subcortically projecting neurons (Hoerder-Suabedissen et al. 2018). Some “silenced” axons in *Drd1a-Cre;Ai14;Snap25<sup>fl/fl</sup>* mice appear fragmented in the striatum and are eventually absent from the thalamus by 8 months of age (Fig. 7H'''). However, by 8–9 months of age, there is no significant reduction in Cre+ cell bodies in L6b of primary somatosensory cortex ( $12.3 \pm 1.4$  [ctrl] vs.  $10.2 \pm 0.8$  [cKO];  $n = 3$  and  $n = 5$  brains respectively, Fig. 7I). All 3 Cre-driver lines have an onset of Cre-expression shortly before or at the time of birth, normal development of projections until P21, but a variable time-course of axonal degeneration, and eventual cell death (see Supplementary Fig. S4 for timeline of various degenerative events).

### Increased Inflammation Accompanies Neurodegeneration

There is evidence of additional inflammatory and degenerative processes occurring in *Rbp4-Cre;Ai14;Snap25<sup>fl/fl</sup>* mice. At 8 months of age, there is a nonsignificant increase in Iba1+ microglia in the cortex of cKO brains compared with controls (Fig. 5B,B') (8 months:  $177 \pm 11$  [ctrl] vs.  $207 \pm 26$  [cKO] cells/mm<sup>2</sup>;  $P = 0.17$  for one-tailed, unequal variance t-test), which is more pronounced in the deepest cortical regions below the *Rbp4-Cre;tdTom+* cell bodies (8 months:  $144 \pm 17$  [ctrl] vs.  $187 \pm 37$  [cKO] cells/mm<sup>2</sup>;  $P = 0.053$  for one-tailed, unequal variance t-test). The density of

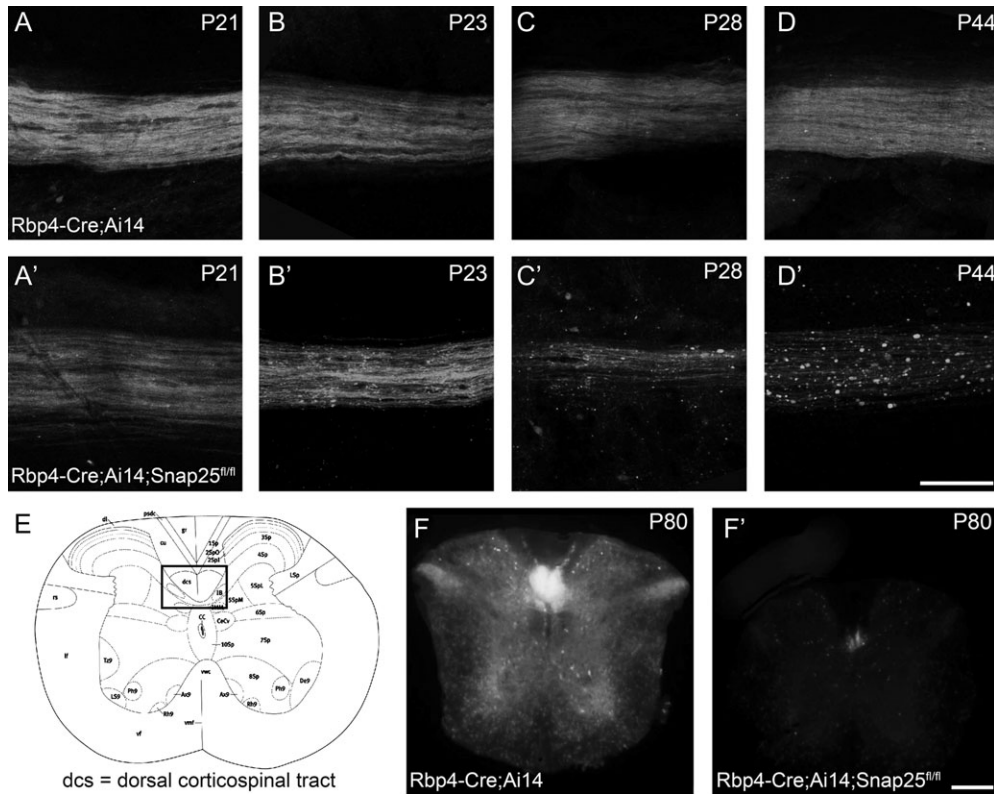


**Figure 3.** Rbp4Cre-mediated excision of *Snap25*<sup>fl/fl</sup> results in axon degeneration in the spinal cord. Laser scanning confocal microscope (A–D) or epifluorescent (F) images of *Rbp4-Cre;Ai14;Snap25*<sup>fl/+</sup> or *Rbp4-Cre;Ai14;Snap25*<sup>fl/fl</sup> brains. (A,A') at P21, the tdTomato+ axons in longitudinal flat-mounts of the dorsal column of spinal cord (cervical level) from *Rbp4-Cre*-expressing corticospinal neurons are indistinguishable in *Rbp4-Cre;Ai14;Snap25*<sup>fl/+</sup> and *Rbp4-Cre;Ai14;Snap25*<sup>fl/fl</sup> mice. (B,B') By P23, the tdTomato+ axons in the dorsal column show the first signs of large swellings in *Rbp4-Cre;Ai14;Snap25*<sup>fl/fl</sup> mice, but not in controls (C,C') by the end of the fourth postnatal week, tdTomato+ axons in the dorsal column are reduced in density and the remaining axons show clear signs of discontinuities and axonal swellings in *Rbp4-Cre;Ai14;Snap25*<sup>fl/fl</sup> mice, but axons in control are indistinguishable from those at P21. (D,D') by P44 no continuous axons are present in the dorsal column of the *Rbp4-Cre;Ai14;Snap25*<sup>fl/fl</sup> mouse, but residual tdTomato+ punctae remain. Control axons remain normal. (E) schematic diagram (Allen Brain Atlas) of the cross-section of the spinal cord at the cervical level, with boxed area indicating the region from which images in panels (F and F') are taken. (F,F') at P80 it is evident in cross-sections of the spinal cord, that there are no tdTomato+ axons remaining in the dorsal column of *Rbp4-Cre;Ai14;Snap25*<sup>fl/fl</sup> mice. Scale bars = 100  $\mu$ m (A–D) and 200  $\mu$ m (F).

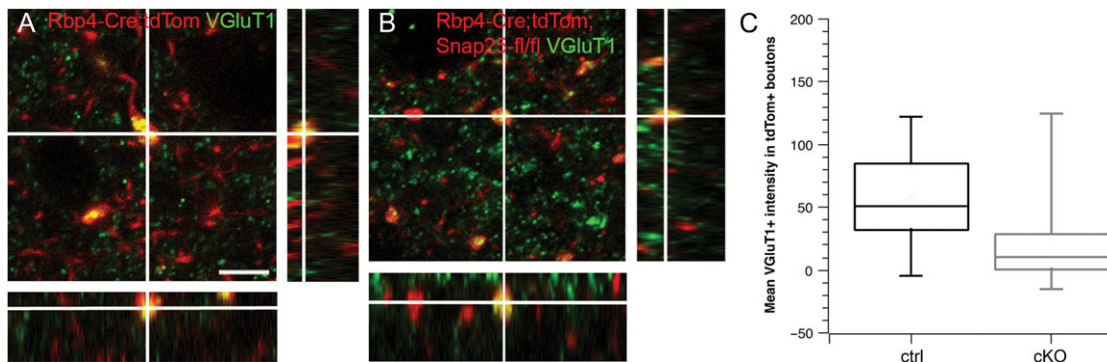


**Figure 4.** Rbp4Cre-mediated excision of *Snap25*<sup>fl/fl</sup> results in reduction of VGLUT1+ synapses from L5 in posterior nucleus (Po) of the thalamus at P28. Single laser scanning confocal images of tdTomato+ structures and VGLUT1+ boutons/punctae in Po thalamus and orthogonal views through the stack of images. (A) VGLUT1+ labels glutamatergic presynaptic terminals of cortical axons projecting to Po thalamus. Both of the large tdTomato+ boutons in Po of *Rbp4-Cre;Ai14* brains are VGLUT1+. (B) VGLUT1+ punctae in Po rarely colocalize with tdTomato+ punctae, but one example is shown. (C) Box-and-whisker plot of the quantification of normalized VGLUT1+ pixel intensity in tdTomato+ presumed boutons in Po. Note, that some boutons in the cKO are as brightly labeled as those in control brains. Considerably more tdTomato+ boutons in the cKO brains are unlabeled with VGLUT1, compared with control brains. Scale bar = 10  $\mu$ m (applies to both panels).

Iba1+ cells was the same in both genotypes at P48 (P48: 210  $\pm$  21 [ctrl] vs. 200  $\pm$  20 [cKO] cells/mm<sup>2</sup> throughout the entire cortical depth). Iba1+ cells with the morphology of activated microglia were mostly identified in cKO brains (1/5 ctrl vs. 5/5 cKO brains at 8 months; 0/3 ctrl vs. 2/3 cKO brains at P48).

In addition to Iba1+ microglia, a general increase in broad-spectrum autofluorescent punctae, probably representing lipofuscin deposits, was evident as a sign of increased inflammation or accelerated ageing. These punctae, shown in green in Figure 5C,C' in 8-month-old brains, fluoresce strongly across



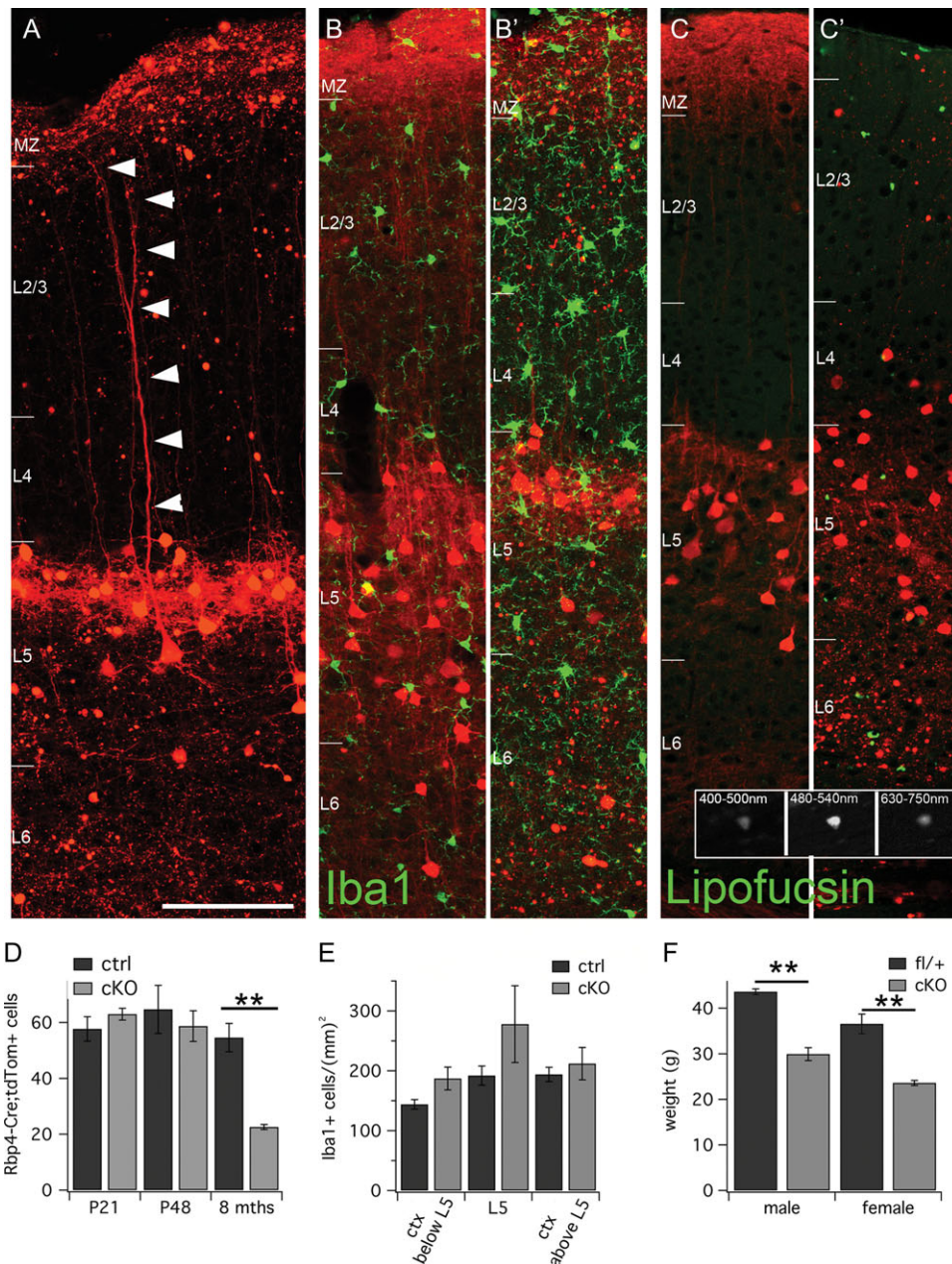


**Figure 5.** Neurodegeneration and inflammation at 8 months of age in “silenced” *Rbp4-Cre* brains. (A–C’) Tiled laser scanning confocal images of 8mth old *Rbp4-Cre; Ai14;Snap25<sup>fl/fl</sup>* and control brains. Cortical layer boundaries are indicated by short horizontal white bars at the left edge of each panel. (A) L5 *Rbp4-Cre;Ai14;Snap25<sup>fl/fl</sup>* cell with an intact dendrite at 8 months of age. (B, B’) Iba1 immunohistochemistry (green) labels more cells in cKO brains (B’) compared with controls (B). (C, C’) Broadband autofluorescence in cKO and control brains (displayed in green) that probably represents lipofuscin deposits is much more prominent in *Rbp4-Cre;Ai14;Snap25<sup>fl/fl</sup>* (C’) brains compared with controls (C). Inset shows greyscale images acquired across a range of wavelengths (indicated at the top of each panel) of one such autofluorescent particle in an 8-month old brain. (D) Quantification of tdTom+ cell body density in L5 of control and cKO brains at P21, P48 and 8 months of age. A significant reduction in cell body density was only evident at 8 months of age in cKO brains. (E) Quantification of Iba1+ cells below L5 (in the region of most axonal degeneration), within L5 (in the region of cell body death) and above L5. There was a nonsignificant increase in Iba1+ cells in all 3 areas in cKO brains at 8 months of age. (F) The body weight of cKO male and female mice is significantly lower in cKO animals (mean age: 32 weeks cKO females, 31 weeks ctrl females and 27 weeks cKO males and 29 weeks ctrl males). For this graph, only fl/fl (cKO) and fl/+ (ctrl) littermates were analyzed. Scale bar = 100  $\mu$ m (applies to all panels, except insets). All measures are mean  $\pm$  s.d.; \*\* $P < 0.01$ . Abbreviations: MZ, marginal zone; L2/3, layer 2/3; L4, layer 4; L5, layer 5; L6, layer 6.

a range of emission spectra (see greyscale inset for emission from 400 to 750 nm). Already at P48 there is a noticeable increase in autofluorescence in cKO brains compared with controls. By 8 months of age this is a significant difference ( $35 \pm 5$  [ctrl] vs.  $100 \pm 24$  [cKO] punctae/425 $\mu$ m-wide cortical column;  $P < 0.01$  for one-tailed, unequal variance t-test).

### *Snap25* cKO in *Rbp4-Cre* Expressing Neurons Results in Limited Behavioral Impairment

*Rbp4-Cre;Snap25<sup>fl/fl</sup>* mice did not show overt physical or behavioral abnormalities at weaning. The genetic ratio of offspring from crosses of *Cre+;Snap25<sup>fl/+</sup>* (female) with *Snap25<sup>fl/fl</sup>* (male) mice was normal, with normal litter size (7.0 pups/litter for

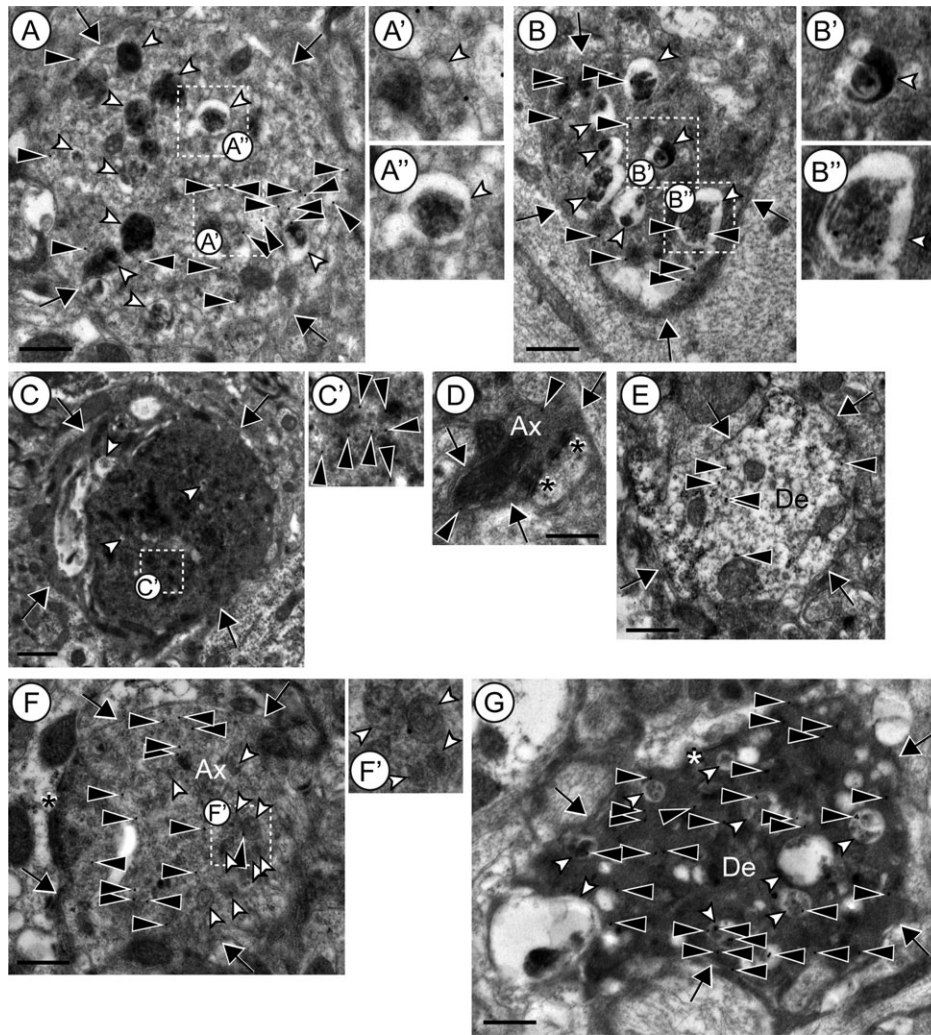


**Figure 6.** Ultrastructure of neurites in cortex of *Rbp4-Cre;Ai14;Snap25<sup>fl/fl</sup>* or *Snap25<sup>fl/fl</sup>* brains at 8 months of age. (A, B) Examples of tdTomato+ neurites containing autophagosome/lysosome-like vacuoles in *Rbp4-Cre;Ai14;Snap25<sup>fl/fl</sup>* cortex. White arrowheads indicate autophagosome/lysosome-like vacuoles. The boxed regions in A and B are enlarged in A', A'' and B', B'', respectively. A' is an example of multivesicular bodies. A'', B' and B'' show vacuoles with an electron-dense body. (C) A typical example of tdTomato+ dystrophic neurites in *Rbp4-Cre;Ai14;Snap25<sup>fl/fl</sup>* that contain electron-dense cytoplasm. The boxed region in C is enlarged in C'. The brightness and contrast of C' were changed to better show immunogold labeling, which is indicated by black arrowheads. (D, E) Representative examples of axonal boutons (D) and dendrites (E) in *Rbp4-Cre;Ai14;Snap25<sup>fl/fl</sup>*. (F) Representative examples of tdTomato+ axonal boutons in *Rbp4-Cre;Ai14;Snap25<sup>fl/fl</sup>*. The boxed region in F is enlarged in F' to show multivesicular bodies in the bouton (white arrowheads). (G) Representative examples of tdTomato+ dendrites with dark cytoplasm in *Rbp4-Cre;Ai14;Snap25<sup>fl/fl</sup>* cortex. Abbreviations: Ax, axon; De, dendrite; arrows indicate the boundary of the boutons or dendrites; filled arrowheads point to tdTomato-immunogold label; open arrowheads indicate multivesicular bodies or vacuoles (see legend above); asterisks indicate postsynaptic densities. Scale bars = 500 nm (A, B, D–G) or 1  $\mu$ m (C).

*Rbp4-Cre;Ai14* and 7.1 pups/litter for *Rbp4-Cre;Ai14;Snap25<sup>fl/fl</sup>* and pup survival. We were unable to use *Rbp4-Cre;Ai14;Snap25<sup>fl/fl</sup>* females for breeding, though, as they consistently abandoned their litters.

With ageing, most cKO animals suspended by their tail show hindlimb clasp (16/21 mice over 30 weeks of age that were monitored for onset of symptoms), but this was never observed during normal handling for *Rbp4-Cre;Ai14;Snap25<sup>fl/fl</sup>* or *Rbp4-Cre;Ai14* mice up to 6 months of age. Onset of first symptoms is usually around 5 months of age.

cKO animals gain body weight more slowly than control animals. At P14–P15, there are no overt differences in body weight ( $8.5 \text{ g} \pm 1$  [ctrl] vs.  $8.7 \text{ g} \pm 0.4$  [cKO];  $n = 6$  ctrl and  $n = 4$  cKO animals of mixed sex). In adult animals, body weight differences are significant (Fig. 5F; female:  $37.0 \text{ g} \pm 2.2$  [fl/+,  $n = 6$ , average age 31 weeks] vs.  $24.0 \text{ g} \pm 0.6$  [fl/fl,  $n = 7$ , average age 32 weeks];

male:  $43.6 \text{ g} \pm 0.6$  [fl/+,  $n = 6$ , average age 29 weeks] vs.  $29.9 \text{ g} \pm 1.4$  [fl/fl,  $n = 3$ , average age 27 weeks]). This is a slowly emerging trend, with minor differences in body weight at 12 weeks of age.

## Discussion

To explore the effect of SNAP25 loss in cortical projection neurons in vivo we have characterized a conditional *Snap25*-KO model (*Rbp4-Cre;Snap25<sup>fl/fl</sup>*). CRE-mediated excision of LoxP-flanked exon5a/b of *Snap25* results in a reduced-length allele and nondetectable protein levels. The majority of evoked release from terminals of cultured hippocampal *Snap25*-cKO neurons is abolished in Cre-recombinase expressing neurons in vitro. The frequency of mIPSCs is reduced in *Snap25*-cKO cultured neurons. Animals with silenced, long-range projecting cortical neuron populations are viable at birth and weaning. In



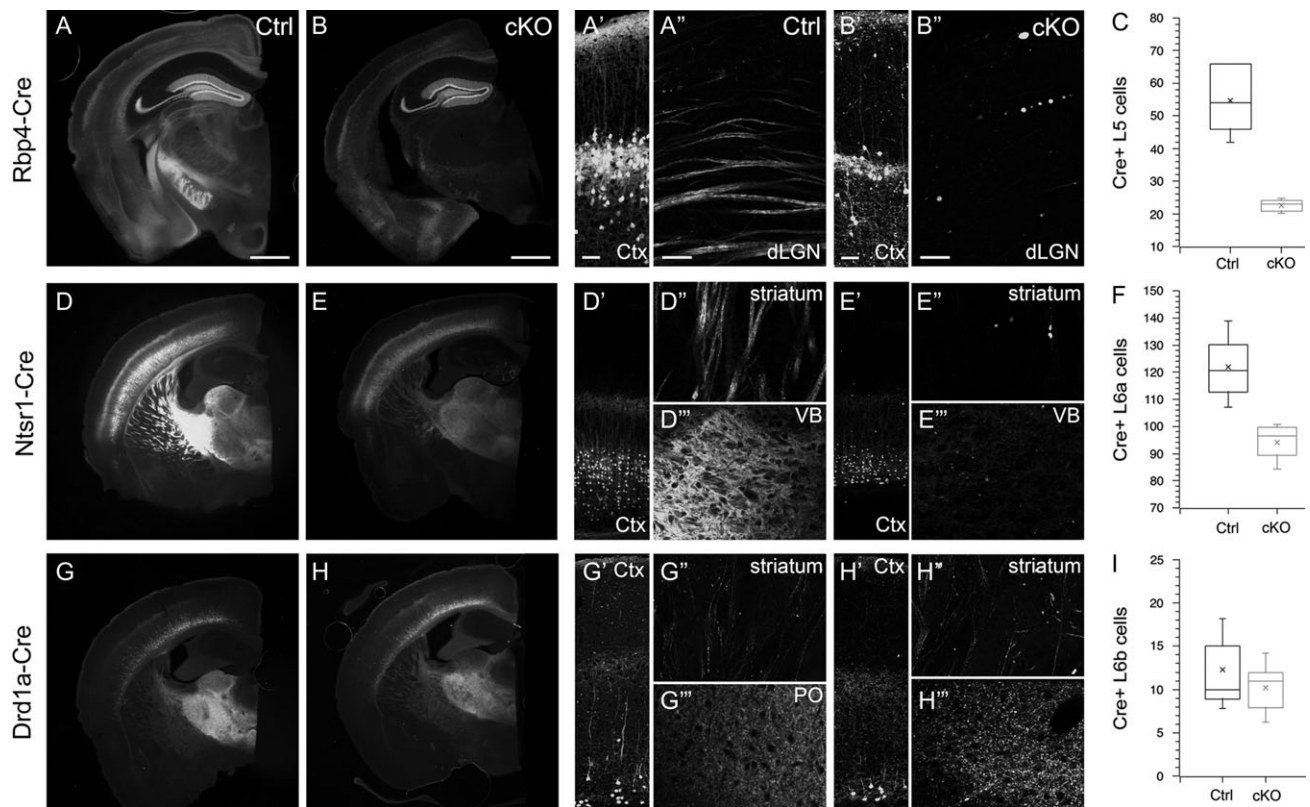


**Figure 7.** Axonal degeneration is present in other cortical Cre-expressing cell populations and shows cell-type specificity in onset and severity. Epifluorescent images of coronal sections of control (Ctrl) and “silenced” (cKO) Rbp4-Cre (A, B), Ntsr1-Cre (D, E) and Drd1a-Cre (G, H) brains, in which Cre-recombinase and tdTomato is expressed in L5, L6 and L6b projection neurons of the cortex respectively. (A', B') Tiled laser-scanning confocal images of cortex highlighting the reduction in cell body density in L5 of cKO brain. (A', B') *Rbp4-Cre;Ai14;Snap25<sup>fl/fl</sup>* results in absence of axons traversing dLGN at 8 months of age. (C) Quantification of total number of Cre+ L5 neurons in cortex of Ctrl and cKO brains. (D', D'', D''') Normal cell density in cortex, intact axons traversing striatum and dense terminal branching in ventrobasal (VB) thalamus of L6 control brains at 8 months of age. (E', E'', E''') *Ntsr1;Ai14;Snap25<sup>fl/fl</sup>* results in reduction of cell bodies in cortical layer 6, and absence of striatal axon bundles and terminal synaptic fields in VB of the thalamus that are prominent in the age-matched control brain. (F) Quantification of total number of Cre+ L6 neurons in cortex of Ctrl and cKO brains. (H', H'', H''') *Drd1a-Cre;Ai14;Snap25<sup>fl/fl</sup>* brains show little reduction in the sparser axon bundles in striatum (H') compared with control (G'), but some large punctae are present in cKO striatum (H''). There is a prominent enlargement of punctae in the terminal synaptic field in posterior nucleus (Po) of the thalamus at 8 months of age (H''') compared with controls (G'''). (I) There is no significant reduction in the number of labeled cell bodies in *Drd1a-Cre;Ai14;Snap25<sup>fl/fl</sup>* brains compared with controls. The time-course of axon degeneration progresses most quickly in L5 axons, at an intermediate pace in L6a axons, but is complete at 8–9 months in both cell populations, but is only beginning in L6b axons by 8 months of age. Images for Rbp4-Cre and Drd1a-Cre are taken at 8 months, images for Ntsr1-Cre are taken at 9–10 months. Scale bars = 1 mm (A, B, D, E, G, H) and 50  $\mu$ m (all other panels). Abbreviations: Ctx, cortex; dLGN, dorsal lateral geniculate nucleus of the thalamus; Po, posterior nucleus of the thalamus; VB, ventrobasal nucleus of the thalamus.

vivo Cre-expression from embryonic stages allows normal development of long-range axonal projections but results in premature axon disintegration in cKO cells and eventual cell death (months after the onset of silencing and loss of axons).

Our results observed in the silenced layer 5 neurons in the *Rbp4-Cre;Snap25<sup>fl/fl</sup>* mouse recapitulate some of the previous observations of the *Snap25* KO, and extend this earlier work to postnatal stages. A reduction in the frequency of spontaneous excitatory synaptic events without reduced amplitude was observed in cell cultures of *Snap25* constitutive KO neurons (Washbourne et al. 2002). Here we additionally report normal amplitude but reduced frequency of GABA-mIPSCs, following *Snap25* cKO in vitro (Supplementary Fig. S3). This confirms a role for SNAP25 in inhibitory neurotransmission during development, as previously suggested by in vivo silencing of SST+ interneurons (Marques-Smith et al. 2016). The residual, spontaneous events observed in the present study and reduction of amplitude but not abolition of evoked transmission may be the result of spontaneous synaptic vesicle fusion which does not require SNAP25 (Washbourne et al. 2002). Most synapses

sampled for presynaptic vesicle fusion events were classified as completely unresponsive, and all neurons in a cell culture assessed for Cre-recombinase expression were CRE+, suggesting that the residual synaptic activity is not a consequence of incomplete Cre-transfection or inefficient excision.

Conditional knockout of *Snap25* in vivo in selected excitatory projection neuron populations of the neocortex and dentate gyrus has no overt developmental or behavioral consequences in young animals. Importantly, a variety of mice with conditional knockout of SNAP25 in the central nervous system were bred producing viable offspring. Here we tested and report the viability of *Rbp4-Cre;Snap25<sup>fl/fl</sup>* (L5), *Drd1a-Cre;Snap25<sup>fl/fl</sup>* (L6b) and *Ntsr1-Cre;Snap25<sup>fl/fl</sup>* (L6) mice, all of which produce viable cKO offspring and had distinct timelines of neurodegenerative processes (Supplementary Fig. S4).

Previous reports using RNAi techniques in cell cultures, implicated SNAP25 in vesicle fusion events necessary for axon outgrowth (Osen-Sand et al. 1993, 1996). Similarly, axon branching has been reported to be severely reduced in *Snap25<sup>-/-</sup>* cell cultures (Delgado-Martinez et al. 2007). Despite this, the central

nervous system develops histologically normally in constitutive SNAP25-KO embryos (Molnár et al. 2002; Washbourne et al. 2002), and also in the more severe Munc18-1 KO in which all neurotransmission is abolished (Verhage et al. 2000; Blakey 2007) and in Munc13 double KO (Blakey 2007) in which both evoked and spontaneous synaptic vesicular release is abolished. Here we confirm that SNAP25 is not required for axon elongation or axon pathfinding in an otherwise normally developing brain, concurring with tissue culture experiments (Blakey et al. 2012) and constitutive KO of SNAP25 or Munc18-1, but contradicting RNAi experiments (Osen-Sand et al. 1993). Axons derived from SNAP25-cKO L5 cells branch and terminate in appropriate higher order thalamic nuclei and grow into the spinal cord, indicating accurate long-range projection targeting. Similarly accurate long-range targeting was also reported for motor neurons forming neuromuscular junctions in Munc18-1 KO embryos (Verhage et al. 2000). However, SNAP25 or intact synaptic transmission is required for the maintenance of these projections. Neurotransmission is essential for axon and cell maintenance after initial synaptic contacts have been established (Verhage et al. 2000). Residual neurotransmitter release observed in SNAP-deficient neurons appears insufficient to ensure cell survival, as cell cultures of SNAP25-deficient neurons have increased cell death after 8–10 days in vitro (DIV) (Washbourne et al. 2002; Delgado-Martínez et al. 2007). Similarly, neurodegeneration occurs from 2 weeks of age in cysteine-string-protein- $\alpha$  (CSP $\alpha$ )-KO mice, in which SNAP25 levels are reduced by 40% (Sharma et al. 2011, 2012). Synapse integrity is severely impaired in CSP $\alpha$ -KO mice, although synapses form normally at first (Fernández-Chacón et al. 2004). In similarity to Munc18-1 KO embryos (Verhage et al. 2000) and Munc18-1 Purkinje cell restricted cKO (Heeroma et al. 2004), syntaxin1a/b dKO embryos (Vardar et al. 2016), and CSP $\alpha$ -KO mice in which SNAP25 levels are reduced (Sharma et al. 2012), but with a much later onset, we observe neurodegeneration in SNAP25-deficient cells in vivo. Here we report in vivo axon degeneration of SNAP25-deficient cells following otherwise normal development. Despite the early loss of axonal integrity, we do not see a reduction in the CRE+, SNAP25-deficient L5 cell population at P48. Significant reduction in Cre+, SNAP25-deficient cells is, however, observed at 8 months of age. This time-course of degenerative processes is much slower than that observed in Munc18-1 KO (midbrain cell loss within 4 days of initial synapse establishment (Verhage et al. 2000)) or CSP $\alpha$ -KO (cell loss within a few weeks of synapse establishment (Sharma et al. 2012)). It is conceivable that the Snap25-cKO neurons described here lack trophic support but are not as severely affected as CSP $\alpha$ -KO neurons because there is unlikely to be an accumulation of misfolded proteins at the synapse. Thus, we conclude that selective Snap25-cKO in some long-range projecting neurons of the central nervous system has no obvious influence on axon pathfinding and initial cell morphology elaboration, but does lead to axonal degeneration and eventual cell death over a time course of months. We also observed a neuronal specific difference between 3 projection neuron populations (layers 5, 6, and 6b), with the larger, and longer-range projecting layer 5 neurons being the most sensitive to the loss of SNAP25 (summarized in Supplementary Fig. S4). Combined with the evidence of very rapid neuronal degeneration following complete silencing of presynaptic neurons in vivo (Munc18-1 KO), and the observation that Munc18-1 KO cell death in cell culture can be delayed by the application of trophic factors such as insulin or BDNF (Heeroma et al. 2004), this suggests that the residual neurotransmitter release in Snap25-cKO can elicit

some trophic feedback, that enables axons to remain intact until the end of the critical period for major pathway reorganization and pruning throughout postnatal development, but is insufficient for long-term maintenance. Moreover, cell-type specific, as yet unidentified factors, are able to delay the onset of axonal degeneration in L6a and L6b cells compared with L5 neurons.

Neurodegeneration in Munc18-1 KO is by apoptotic mechanisms, accompanied by a general increase in activated macrophages (Verhage et al. 2000). Here we attempted to demonstrate similar apoptotic mechanisms using antiactivated Caspase 3 immunohistochemistry (data not shown), but could not observe apoptotic features in the cerebral cortex at 8 months of age. Similarly, we did not observe nuclei containing condensed chromatin in cortex of 8-month-old *Rpb4-Cre;Ai14;Snap25<sup>fl/fl</sup>* mice. This might be because the cell death occurs over a very protracted time, compared with the rapid degeneration observed in Munc18-1 KO. Additional studies have compared cell death of Munc18-1 KO, t-SNARE and v-SNARE-depleted neuronal cell cultures. Munc18-1 and t-SNAREs (including SNAP-25) are essential for neuronal survival in culture, whereas v-SNAREs are not (Santos et al. 2017). Neuronal death in culture is preceded by condensation of the Golgi apparatus that is distinct from the fragmentation seen during apoptosis (Santos et al. 2017). We did not assess Golgi apparatus morphology on our EM images of cortex of 8-month-old *Rpb4-Cre;Ai14;Snap25<sup>fl/fl</sup>* mice.

Dystrophic neurites with dark cytoplasm were observed by electron microscopy in *Rbp4-Cre;Ai14;Snap25<sup>fl/fl</sup>* cortex of mice aged 8 months. Darkening of cytoplasm is a known feature of axons undergoing degeneration (Baumgarten et al. 1974; Saggu and Chotaliya 2010). The dystrophic neurites likely correspond to large tdTomato-positive swellings in the *Snap25<sup>fl/fl</sup>* cortex. Many of those swellings are assumed to derive from axons and presynaptic terminals, and immuno-electron microscopy confirmed the presence of tdTomato-positive dystrophic presynaptic boutons in the *Snap25<sup>fl/fl</sup>* cortex. An increase in the size of presynaptic terminals was also observed in the striatum of *Snap25<sup>S187A/S187A</sup>* mutant mice, in which the S187 residue of SNAP25 is unphosphorylatable and neurotransmitter release is decreased (Nakata et al. 2012). Here we report accumulations of autophagosome/lysosome-like vacuoles in *Rbp4-Cre;Snap25<sup>fl/fl</sup>*; Ai14 neurites. These structures are similar to those observed in mouse models of Alzheimer's disease (Masliah et al. 1996; Sanchez-Varo et al. 2012), where dystrophic neurites show a variety of morphology, size and cytoplasmic alterations. The similarity in the cytoplasmic features of dystrophic neurites between *Rbp4-Cre;Ai14;Snap25<sup>fl/fl</sup>* and Alzheimer's disease models, suggests that they share, at least partially, degenerative processes. Electron microscopic observation of the brains of patients with Alzheimer's disease have also shown that autophagy-lysosome pathways are linked to neurite degeneration in the cerebral cortex (Nixon et al. 2005; Blazquez-Llorca et al. 2010; Nixon 2013; Yang et al. 2013).

Here we show an example of a surviving L5 neurons in *Rbp4-Cre;Ai14;Snap25<sup>fl/fl</sup>* cortex which has an intact, and elaborate dendrite as appropriate for a L5 pyramidal neuron. Previously, it has been shown that dendrites including spines initially form normally in cell cultures with abolished neurotransmission (Munc13 double knock-out (Varoqueaux et al. 2002; Sigler et al. 2017)). However, Sando et al. (2017) report a reduction in dendrite length for CA3 and cortical pyramidal neurons but not dentate gyrus granule cells in transgenic mice without glutamatergic neurotransmission (*Emx1<sup>IRRES-Cre</sup>*; *R26<sup>flxstop</sup>TeNT*) (Sando et al. 2017)). We acknowledge that

“silenced” L5 pyramidal neurons might have similar defects, but owing to the high density of labeled cells in the brains prior to the onset of cell loss, single cell dendritic reconstructions were beyond the scope of this study.

*Bdr* mice show characteristic ataxic gait and prepulse inhibition deficits (Jeans et al. 2007), and Coloboma (Cb/+) mice are spontaneously hyperactive (Hess et al. 1996). Here we report no obvious behavioral phenotype in young *Rbp4-Cre;Snap25<sup>fl/fl</sup>;Ai14* mice, except for a consistent reduction in weight gain, which might be indicative of hyperactivity.

In conclusion, we present evidence of the effective presynaptic silencing of selected groups of neurons in vitro and in vivo using the *Snap25<sup>fl/fl</sup>* mouse. This mouse model may be useful to elucidate the contribution of different brain regions and/or cell types to rodent models of psychiatric disease. Over short time-scales, it is also ideally suited to eliminate individual elements of the cortical circuitry to assess their overall contribution, without the attendant inflammatory response inherent to acute cell ablation experiments, as we observed no increase in inflammatory processes at P48. Lastly, it may be a suitable tool to investigate slowly progressing axon degeneration, associated myelin defects and neurodegeneration and the stress this places on the remaining circuit and neighboring cells or axons in vivo. This would also allow for testing of environmental factors influencing such processes.

## Supplementary Material

Supplementary material is available at *Cerebral Cortex* online.

## Funding

Medical Research Council (UK) (Grants G00900901: “Formation of the earliest circuits in the cerebral cortex” and MR/N026039/1: “Role of Neurosecretion in early cortical circuit formation”). S.H. was supported from Daiichi Sankyo Foundation of Life Science, Japan.

## Notes

This article is dedicated to the memory of our colleague and friend Professor Michael C. Wilson, who died unexpectedly towards the end of 2014. We gratefully acknowledge assistance with tissue cutting and immunohistochemistry from Dr Kristina Parley and Ms Sanskrithi Sravanam. *Conflict of Interest:* None declared.

## References

Ayalew M, Le-Niculescu H, Levey DF, Jain N, Changala B, Patel SD, Winiger E, Breier A, Shekhar A, Amdur R, et al. 2012. Convergent functional genomics of schizophrenia: from comprehensive understanding to genetic risk prediction. *Mol Psychiatry*. 17:887–905.

Baca M, Allan AM, Partridge LD, Wilson MC. 2013. Gene-environment interactions affect long-term depression (LTD) through changes in dopamine receptor affinity in *Snap25* deficient mice. *Brain Res*. 1532:85–98.

Baumgarten HG, Björklund A, Horn AS, Schlossberger HG. 1974. Dynamics of degeneration and growth in neurons, dynamics of degeneration and growth in neurons. New York: Pergamon Press.

Berczki E, Francis PT, Howlett D, Pereira JB, Höglund K, Bogstedt A, Cedazo-Minguez A, Baek J-H, Hortobágyi T, Attems J, et al. 2016. Synaptic proteins predict cognitive

decline in Alzheimer’s disease and Lewy body dementia. *Alzheimers Dement*. 12:1149–1158.

Blakey D. 2007. The role of neural activity in the development of thalamocortical connections [DPhil thesis]. University of Oxford.

Blakey D, Wilson MC, Molnár Z. 2012. Termination and initial branch formation of SNAP-25-deficient thalamocortical fibres in heterochronic organotypic co-cultures. *Eur J Neurosci*. 35:1586–1594.

Blazquez-Llorca L, Garcia-Marin V, DeFelipe J. 2010. GABAergic complex basket formations in the human neocortex. *J Comp Neurol*. 518:4917–4937.

Bronk P, Deák F, Wilson MC, Liu X, Südhof TC, Kavalali ET. 2007. Differential effects of SNAP-25 deletion on Ca2+ -dependent and Ca2+ -independent neurotransmission. *J Neurophysiol*. 98:794–806.

Dai D, Wang Y, Yuan J, Zhou X, Jiang D, Li J, Zhang Y, Yin H, Duan S. 2014. Meta-analyses of 10 polymorphisms associated with the risk of schizophrenia. *Biomed Reports*. 2: 729–736.

Delgado-Martínez I, Nehring RB, Sørensen JB. 2007. Differential abilities of SNAP-25 homologs to support neuronal function. *J Neurosci*. 27:9380–9391.

Faraone SV, Khan SA. 2006. Candidate gene studies of attention-deficit/hyperactivity disorder. *J Clin Psychiatry*. 67 (Suppl 8):13–20.

Fernández-Chacón R, Wölfel M, Nishimune H, Tabares L, Schmitz F, Castellano-Muñoz M, Rosenmund C, Montesinos ML, Sanes JR, Schneggenburger R, et al. 2004. The synaptic vesicle protein CSP alpha prevents presynaptic degeneration. *Neuron*. 42:237–251.

Garcia-Reitböck P, Anichtchik O, Bellucci A, Iovino M, Ballini C, Fineberg E, Ghetti B, Della Corte L, Spano P, Tofaris GK, et al. 2010. SNARE protein redistribution and synaptic failure in a transgenic mouse model of Parkinson’s disease. *Brain*. 133: 2032–2044.

Gong S, Doughty M, Harbaugh CR, Cummins A, Hatten ME, Heintz N, Gerfen CR. 2007. Targeting Cre recombinase to specific neuron populations with bacterial artificial chromosome constructs. *J Neurosci*. 27:9817–9823.

Grant E, Hoerder-Suabedissen A, Molnár Z. 2016. The regulation of corticofugal fiber targeting by retinal inputs. *Cereb Cortex*. 26:1336–1348.

Groh A, Bokor H, Mease RA, Plattner VM, Hangya B, Stroh A, Deschenes M, Acsády L. 2014. Convergence of cortical and sensory driver inputs on single thalamocortical cells. *Cereb Cortex*. 24:3167–3179.

Heeroma JH, Roelandse M, Wierda K, Van Aerde KI, Toonen RFG, Hensbroek RA, Brussaard A, Matus A, Verhage M. 2004. Trophic support delays but not prevent cell-intrinsic degeneration of neurons deficient for *munc18-1*. *Eur J Neurosci*. 20:623–634.

Hess EJ, Collins KA, Wilson MC. 1996. Mouse model of hyperkinesis implicates SNAP-25 in behavioral regulation. *J Neurosci*. 16:3104–3111.

Hess EJ, Jinnah HA, Kozak CA, Wilson MC. 1992. Spontaneous locomotor hyperactivity in a mouse mutant with a deletion including the *Snap* gene on chromosome 2. *J Neurosci*. 12: 2865–2874.

Hoerder-Suabedissen A, Hayashi S, Upton L, Zachary N, Casas-Torremocha D, Eleanor G, Sarada V, Kanold PO, Fracisco C, Kim Y, et al. 2018. Subset of cortical layer 6b neurons selectively innervates higher order thalamic nuclei in mice. *Cereb Cortex*. 28:1882–1897.



- Hoogland PV, Wouterlood FG, Welker E, Van der Loos H. 1991. Ultrastructure of giant and small thalamic terminals of cortical origin: a study of the projections from the barrel cortex in mice using Phaseolus vulgaris leuco-agglutinin (PHA-L). *Exp Brain Res*. 87:159–172.
- Jean AF, Oliver PL, Johnson R, Capogna M, Vikman J, Molnár Z, Babbs A, Partridge CJ, Salehi A, Bengtsson M, et al. 2007. A dominant mutation in Snap25 causes impaired vesicle trafficking, sensorimotor gating, and ataxia in the blind-drunk mouse. *Proc Natl Acad Sci U S A*. 104:2431–2436.
- Kishi-Itakura C, Koyama-Honda I, Itakura E, Mizushima N. 2014. Ultrastructural analysis of autophagosome organization using mammalian autophagy-deficient cells. *J Cell Sci*. 127:4984–4984.
- Lamprecht MR, Sabatini DM, Carpenter AE. 2007. CellProfiler: free, versatile software for automated biological image analysis. *Biotechniques*. 42:71–75.
- Marques-Smith A, Lyngholm D, Kaufmann A-K, Stacey JA, Hoerder-Suabedissen A, Becker EBE, Wilson MC, Molnár Z, Butt SJB. 2016. A transient transaminar GABAergic interneuron circuit connects thalamocortical recipient layers in neonatal somatosensory cortex. *Neuron*. 89:536–549.
- Masliah E, Sisk A, Mallory M, Mucke L, Schenk D, Games D. 1996. Comparison of neurodegenerative pathology in transgenic mice overexpressing V717F beta-amyloid precursor protein and Alzheimer's disease. *J Neurosci*. 16:5795–5811.
- Molnár Z, López-Bendito G, Small J, Partridge LD, Blakemore C, Wilson MC. 2002. Normal development of embryonic thalamocortical connectivity in the absence of evoked synaptic activity. *J Neurosci*. 22:10313–10323.
- Nakata Y, Yasuda T, Fukaya M, Yamamori S, Itakura M, Nihira T, Hayakawa H, Kawanami A, Kataoka M, Nagai M, et al. 2012. Accumulation of  $\alpha$ -synuclein triggered by presynaptic dysfunction. *J Neurosci*. 32:17186–17196.
- Nixon RA. 2013. The role of autophagy in neurodegenerative disease. *Nat Med*. 19:983–997.
- Nixon RA, Wegiel J, Kumar A, Yu WH, Peterhoff C, Cataldo A, Cuervo AM. 2005. Extensive involvement of autophagy in Alzheimer disease: an immuno-electron microscopy study. *J Neuropathol Exp Neurol*. 64:113–122.
- Oliver PL, Sobczyk MV, Maywood ES, Edwards B, Lee S, Livieratos A, Oster H, Butler R, Godinho SIH, Wulff K, et al. 2012. Disrupted circadian rhythms in a mouse model of schizophrenia. *Curr Biol*. 22:314–319.
- Olsen SR, Bortone DS, Adesnik H, Scanziani M. 2012. Gain control by layer six in cortical circuits of vision. *Nature*. 483:47–52.
- Osen-Sand A, Catsicas M, Staple JK, Jones KA, Ayala G, Knowles J, Grenningloh G, Catsicas S. 1993. Inhibition of axonal growth by SNAP-25 antisense oligonucleotides in vitro and in vivo. *Nature*. 364:445–448.
- Osen-Sand A, Staple JK, Naldi E, Schiavo G, Rossetto O, Petitpierre S, Malgaroli A, Montecucco C, Catsicas S. 1996. Common and distinct fusion proteins in axonal growth and transmitter release. *J Comp Neurol*. 367:222–234.
- Rizo J, Südhof TC. 2012. The membrane fusion enigma: SNAREs, Sec1/Munc18 proteins, and their accomplices—guilty as charged? *Annu Rev Cell Dev Biol*. 28:279–308.
- Saggu SK, Chotaliya HP. 2010. Wallerian-like axonal degeneration in the optic nerve after. *BMC Neurosci*. 11:97.
- Sanchez-Varo R, Trujillo-Estrada L, Sanchez-Mejias E, Torres M, Baglietto-Vargas D, Moreno-Gonzalez I, De Castro V, Jimenez S, Ruano D, Vizuete M, et al. 2012. Abnormal accumulation of autophagic vesicles correlates with axonal and synaptic pathology in young Alzheimer's mice hippocampus. *Acta Neuropathol*. 123:53–70.
- Sando R, Bushong E, Zhu Y, Huang M, Considine C, Phan S, Ju S, Uytiepo M, Ellisman M, Maximov A. 2017. Assembly of excitatory synapses in the absence of glutamatergic neurotransmission. *Neuron*. 94:312–321.e3.
- Santos TC, Wierda K, Broeke JH, Toonen RF, Verhage M. 2017. Early golgi abnormalities and neurodegeneration upon loss of presynaptic proteins Munc18-1, Syntaxin-1, or SNAP-25. *J Neurosci*. 37:4525–4539.
- Sharma M, Burré J, Bronk P, Zhang Y, Xu W, Südhof TC. 2012. CSP $\alpha$  knockout causes neurodegeneration by impairing SNAP-25 function. *EMBO J*. 31:829–841.
- Sharma M, Burré J, Südhof TC. 2011. CSP $\alpha$  promotes SNARE-complex assembly by chaperoning SNAP-25 during synaptic activity. *Nat Cell Biol*. 13:30–39.
- Sigler A, Oh WC, Imig C, Altas B, Kawabe H, Cooper BH, Kwon HB, Rhee JS, Brose N. 2017. Formation and maintenance of functional spines in the absence of presynaptic glutamate release. *Neuron*. 94:304–311.e4.
- Vardar G, Chang S, Arancillo M, Wu Y-J, Trimbuch T, Rosenmund C. 2016. Distinct functions of Syntaxin-1 in neuronal maintenance, synaptic vesicle docking, and fusion in mouse neurons. *J Neurosci*. 36:7911–7924.
- Varoqueaux F, Sigler A, Rhee J-S, Brose N, Enk C, Reim K, Rosenmund C. 2002. Total arrest of spontaneous and evoked synaptic transmission but normal synaptogenesis in the absence of Munc13-mediated vesicle priming. *Proc Natl Acad Sci*. 99:9037–9042.
- Verhage M, Maia AS, Plomp JJ, Brussaard AB, Heeroma JH, Vermeer H, Toonen RF, Hammer RE, Van Den Berg TK, Missler M, et al. 2000. Synaptic assembly of the brain in the absence of neurotransmitter secretion. *Science*. 287:864–869.
- Washbourne P, Thompson PM, Carta M, Costa ET, Mathews JR, Lopez-Bendito G, Molnár Z, Becher MW, Valenzuela CF, Partridge LD, et al. 2002. Genetic ablation of the t-SNARE SNAP-25 distinguishes mechanisms of neuroexocytosis. *Nat Neurosci*. 5:19–26.
- Yang Y, Coleman M, Zhang L, Zheng X, Yue Z. 2013. Autophagy in axonal and dendritic degeneration. *Trends Neurosci*. 36:418–428.